https://doi.org/10.5194/egusphere-2025-1763
Preprint. Discussion started: 10 June 2025
© Author(s) 2025. CC BY 4.0 License.

Assessing sea level rise and extreme events along the China-Europe Sea Route

Rita Lecci[1], Robyn Gwee[2,3,4], Kun Yan[2], Sanne Muis[2,5], Nadia Pinardi[6,1], Jun She[7], Martin Verlaan[2], Simona Masina[1], Wenshan Li[8], Hui Wang[8], Salvatore Causio[1], Antonio Novellino[9], Marco Alba[9], Etiënne Kras[2], Sandra Gaytan Aguilar[2], Jan-Bart Calewaert[10,11]

[1] CMCC Foundation – Euro-Mediterranean Centre on Climate Change, Italy
[2] Marine & Coastal Systems Unit, Deltares, Delft, The Netherlands
[3] Centre for Nature-based Climate Solutions, National University of Singapore, Singapore, Singapore
[4] Department of Biological Sciences, National University of Singapore, Singapore, Singapore
[5] Institute for Environmental Studies (IVM), Vrije Universiteit Amsterdam, Amsterdam, The Netherlands
[6] Department of Physics and Astronomy, University of Bologna, Bologna, Italy
[7] Department of Weather Research, Danish Meteorological Institute, Copenhagen, Denmark
[8] National Marine Data and Information Service (NMDIS), Tianjin, China
[9] ETT SpA, Genova, Italy
[10] Secretariat of the European Marine Observation and Data Network (EMODnet), Ostend, Belgium
[11] Seascape Belgium, Brussels, Belgium

Correspondence to: Rita Lecci (rita.lecci@cmcc.it)

Abstract. The Intergovernmental Panel on Climate Change (IPCC) Sixth Assessment Report highlights the critical acceleration of global mean sea level (GMSL) rise, with trends surpassing historical rates observed over the past two millennia. The China-Europe Sea Route (CESR), a region of strategic importance for international trade, is particularly vulnerable to sea level changes and extreme events. This study integrates satellite altimetry, tide gauge records, and advanced hydrodynamic models to assess absolute and relative sea level variations, as well as extreme sea level events, across eight CESR sub-regions over the period 1993–2023.

Statistically significant mean sea level trends confirm consistent and systematic changes in sea level trends by decade and across regions. Notably the East China Sea, Yellow Sea and Bohai Sea show a decadal trend slowdown in the second (2003-2023) and third decade (2013-2023) with respect to the first one (1993-2003).

Accelerated regional mean SLA trends are observed in the North Indian Ocean, while Pacific sub-regions exhibited decadal variability. Discrepancies between tide gauge and satellite data in specific areas were attributed to land subsidence and inherent limitations of coastal altimetry.

Numerical modeling using the Global Tide and Surge Model (GTSM) provided estimates of return periods for extreme sea levels, identifying high-risk zones such as the Bay of Bengal and the South China Sea. However, challenges remain in capturing cyclone impacts, emphasizing the need for improved modeling frameworks.

By highlighting the importance of localized, data-driven approaches and continuous monitoring, the findings contribute to advancing climate resilience and informing risk mitigation strategies in this globally significant region.

https://doi.org/10.5194/egusphere-2025-1763
Preprint. Discussion started: 10 June 2025
© Author(s) 2025. CC BY 4.0 License.

1 Introduction

The Intergovernmental Panel for Climate Change (IPCC) Sixth Assessment Report (AR6), published in 2021, revealed unprecedented changes in the global climate system over the past two centuries (1850–2020) (IPCC, 2021). During this period, significant transformations have occurred in heat, water, and ice dynamics across various climate compartments. Among these changes, the global mean sea level (GMSL) rise stands out as a critical indicator, reflecting the interplay of complex climate processes. Since the mid-19th century, the GMSL has accelerated beyond the average rate observed over the past two millennia. Between 1901 and 2018, the GMSL rose by 0.20 m, with the rate increasing from 1.3 mm/yr (1901–1971) to 3.7 mm/yr (2006–2018). Satellite altimetry data further confirm this acceleration, estimating it at 0.084 ± 0.025 mm/yr² between 1993 and 2018 (Nerem et al., 2018).

The primary drivers of GMSL changes include the melting of polar ice sheets, land glaciers, and ocean thermal expansion. Notably, the Antarctic ice sheet's mass loss tripled, and the Greenland ice sheet's mass loss doubled between the periods 1997–2006 and 2007–2016. Interannual variability in the water cycle can temporarily slow the trend of mean sea level rise, as observed in the global ocean from 2003 to 2011 (Cazenave et al., 2014) and in the Mediterranean Sea between 2013 and 2022 (Borile et al., 2025). These findings highlight the influence of short-term climate variability on sea level trends, which is not limited to the global scale but also affects regional seas and localized oceanic areas. Additionally, regional sea level changes are shaped by local ocean circulation patterns, underlining the need for detailed studies of regional and coastal dynamics (Ezer et al., 2013; Pinardi et al., 2014, Dangendorf, 2021).

The North Indian Ocean, identified in the IPCC WG1 report, has experienced sea level rise faster than the global average, leading to coastal area loss and shoreline retreat. This region, encompassing the China-Europe Sea Route (CESR), is of particular interest due to its importance for international trade. However, capturing the full complexity of regional sea level changes in such areas requires high-resolution, locally refined datasets that go beyond the scope of global assessments.

Efforts to monitor sea level trends on regional and global scales have been bolstered by initiatives such as the Copernicus Marine Service (CMEMS). Since 2016, CMEMS has published annual Ocean State Reports (OSR), which focus on "Ocean Monitoring Indicators" (OMI), including sea level rise. These reports provide a comprehensive overview of the global ocean and regional European Seas, addressing key variables, climate change impacts, natural variability, and extreme events. Furthermore, a European Assessment Report on Sea Level Rise has been developed for all European basins utilizing a co-designed approach with policymakers and grounded in robust scientific methods (van den Hurk et al., 2024).

In China, complementary initiatives such as the 'China Sea Level Bulletin' and the 'China Marine Hazards Bulletin,' both launched in 2003, provide annual insights into sea level trends and marine hazards. The former focuses on the annual mean sea level rise along the Chinese coast, including related coastal hazards, while the latter addresses a broader spectrum of marine hazards and their socioeconomic implications.

This study builds on these efforts, employing local and previously unexamined datasets, including Satellite Altimetry (SLA) data, to deliver a more accurate and high-resolution regional assessment of the CESR region. By integrating high-quality local

https://doi.org/10.5194/egusphere-2025-1763
Preprint. Discussion started: 10 June 2025
© Author(s) 2025. CC BY 4.0 License.

data with global datasets, this work seeks to provide a detailed analysis of sea level variability, trends, and extreme events in the region. These findings extend the conclusions of AR6, leveraging the best available, quality-controlled historical data alongside high-resolution sea level climate projections.

The paper begins with an overview of observational sea level rise data, followed by insights from numerical model outputs. Section 2 outlines the materials and methods, including the novel integration of SLA and local datasets. Section 3 presents an analysis of absolute and relative sea level changes, with a particular focus on extreme sea level events in the CESR region. The paper concludes with a discussion of the findings and their implications for regional coastal risk assessments and adaptation strategies.

2 Material and methods

This section describes the datasets, models, and methodologies employed to analyze sea level changes and extreme sea level events in the China-Europe Sea Route (CESR) region.

2.1 Datasets

This study integrates a range of data sources, including satellite altimetry, tide gauge measurements, and advanced numerical models, to comprehensively assess sea level dynamics.

The global sea level product from the Copernicus Marine Service (CMEMS) serves as the primary dataset for absolute sea level analysis. The product used for the analysis is provided by CMEMS with nomenclature SEALEVEL_GLO_PHY_CLIMATE_L4_MY_008_057. Derived from multiple satellite altimetry missions and processed through the DUACS system (https://duacs.cls.fr), this dataset offers daily gridded Level 4 data with a spatial resolution of 0.25° (~25 km), spanning the global ocean from 1993 to 2023. The current version, DUACS Delayed-Time DT-2024, is referenced to a 20-year baseline (1993–2012). To address the challenges of satellite altimetry near coastlines, wet tropospheric corrections are applied within 20–50 km of the coast. For this study, monthly mean anomalies, where the mean monthly seasonal cycle was removed, were used to analyze trends over the 1993–2023 period.

Relative sea level data were obtained from the Revised Local Reference (RLR) dataset provided by the Permanent Service for Mean Sea Level (PSMSL) (https://psmsl.org/data/obtaining/complete.php). The RLR dataset standardizes tide gauge records to a common reference datum, simplifying the analysis of time series while eliminating negative values. The common reference level is set at 7000 mm below mean sea level. For this study, tide gauge records from 1993 onward were selected to validate satellite altimetry data and investigate the impacts of land movement, such as subsidence.

While tide gauges provide high-resolution, localized measurements of relative sea level, satellite altimetry offers a broader synoptic view of absolute sea level. This complementary relationship allows for the validation of coastal altimetry data, which are prone to higher uncertainties near shorelines due to land contamination and reduced resolution (Zhou et al., 2020). Altimetry corrections, such as those for wet tropospheric effects, become inaccurate within 20–50 km of the coast, leading to

https://doi.org/10.5194/egusphere-2025-1763
Preprint. Discussion started: 10 June 2025
© Author(s) 2025. CC BY 4.0 License.

reduced data quality in these areas. Coastal-specific altimetry products that address these challenges are not yet available for the entire 1993–2023 period (Zhou et al., 2020; Climate Change Initiative Coastal Sea Level Team, 2020).

The comparison of tide gauge and satellite data is particularly important for the CESR region, which exhibits diverse circulation patterns, monsoonal influences, and significant contributions from steric effects, glacial isostatic adjustment (GIA), and land subsidence. For example, along China's eastern coast, subsidence rates of a few millimeters per year have been identified in areas like the Yangtze River delta, while negligible subsidence has been observed along the Guangdong and Liaoning coasts (Xue et al., 2005; Zhu et al., 2015). However, GIA models often fail to capture these local subsidence signals (Schumacher et al., 2018).

Extreme sea level events were analyzed using the Global Tide and Surge Model (GTSM) (Muis et al., 2016), a hydrodynamic model implemented through the Delft3D Flexible Mesh software. GTSM operates at variable resolutions, ranging from 1.25 km near coasts to 30 km offshore (Fig. A1). Two specific datasets were utilized: GTSMip (Global Tide and Surge Model Intercomparison Project) (Muis et al., 2022) and COAST-RP (Coastal dAtaset of Storm Tide Return Periods) (Dullaart et al., 2021). GTSMip is based on GTSMv3.0 and ERA5 reanalysis data (Hersbach et al., 2020), estimates return periods using the Peaks Over Threshold method, applying a Generalized Pareto Distribution (GPD) fitted through Maximum Likelihood Estimation. COAST-RP combines synthetic tropical cyclone tracks representing 10,000 years of activity with ERA5 reanalysis data to refine return period estimates in cyclone-prone regions. However, GTSM tends to underestimate extreme sea levels due to ERA5's underestimation of storm winds, a key driver of extreme events. This limitation underscores the importance of incorporating observational data and additional regional models to validate and enhance results.

Tide gauge data from the University of Hawaii Sea Level Center (UHSLC) were used to validate return period estimates derived from GTSM. These records, spanning over 25 years with minimal missing data, ensure a robust comparison with modeled extreme events.

By integrating these diverse datasets, the study achieves a comprehensive evaluation of sea level variability, trends, and extreme events with enhanced spatial and temporal resolution.

2.2 Methodology

The methodology combines observational data analysis and numerical modeling to evaluate both absolute and relative sea level trends, along with extreme events, in the CESR region.

Satellite monthly mean anomaly sea level data for CESR sub-regions were used to compute linear trends over the past three decades. These trends have been fitted using linear regression, allowing comparisons with global averages to identify spatial variability across sub-regions. The statistical significance of the trends was assessed, and the associated standard errors were calculated to quantify uncertainties. Tide gauge data were corrected for land movement using Glacial Isostatic Adjustment (GIA) models and GPS data. These corrections ensure that local land subsidence effects are accurately captured. Comparisons between tide gauge measurements and nearby satellite altimetry grid points assess consistency, especially near coastlines where land movement may distort sea level measurements.

https://doi.org/10.5194/egusphere-2025-1763
Preprint. Discussion started: 10 June 2025
© Author(s) 2025. CC BY 4.0 License.

GTSMv3 is a depth-averaged hydrodynamic model with global coverage, based on the Delft3D Flexible Mesh software with spatially varying resolution that increases towards the coast (Figure 15, from 30km resolution in the deep ocean to 1.25km along the coast). GTSMip is based on GTSMv3.0 and ERA5, with return periods derived following the Peaks Over Threshold (POT) method by fitting a Gumbel distribution to the annual maxima. A Generalized Pareto Distribution (GPD) is fitted to the independent peaks exceeding the 99th percentile. The GPD is parameterized by shape, location and scale parameters obtained following Maximum Likelihood Estimation (MLE). The starting estimate for the fit of the shape parameter is set to 0 to minimize the effect of outliers. Uncertainty bounds are derived using bootstrapping with 599 repetitions.

COAST-RP dataset contains improved estimation of return periods for regions prone to tropical cyclones (Dullaart et al., 2021). The amplitude of tropical cyclones can be underestimated by ERA5 (Dullaart et al., 2020), in addition to the infrequent occurrence of tropical cyclones and a limited tropical cyclone dataset of only 40 years. This makes it difficult to reliably estimate return periods. To address this, Bloemendaal et al. (2020) generated a synthetic tropical cyclone track representing 10,000 years of tropical cyclone conditions, which was incorporated into the COAST-RP dataset. Return periods of different water levels are derived by making an estimation of empirical probabilities using the Weibull plotting formulations instead of EVA.

Extreme sea level events were assessed using Extreme Value Analysis (EVA) techniques applied to GTSM data. Gumbel and Generalized Pareto Distributions (GPD) were used to estimate return periods for high-water events, with a particular focus on 1-in-100-year occurrences. Independent peak values, separated by at least 72 hours, were extracted from tide gauge data for validation purposes.

Spatial mapping of sea level trends across the CESR region highlights areas experiencing higher rates of change, particularly in zones influenced by strong currents or local subsidence. Additional maps of Mean High Higher Water (MHHW) and the Highest Astronomical Tide (HAT) clarify tidal contributions to extreme sea level events.

GTSMip and COAST-RP datasets provide insights into extreme events, but are limited by short reanalysis periods, particularly in cyclone-prone areas. Synthetic cyclone tracks were integrated to refine return period estimates in these regions, addressing the challenges posed by ERA5's storm wind underestimation.

This integrated approach effectively captures both gradual and extreme sea level changes, providing a robust framework for assessing variability and risk in the CESR region. The findings inform strategies for enhancing coastal resilience and risk management.

https://doi.org/10.5194/egusphere-2025-1763
Preprint. Discussion started: 10 June 2025
© Author(s) 2025. CC BY 4.0 License.

3 Results

3.1 Sea level trend

3.1.1 Absolute sea level

Eight distinct sub-regions within the China-Europe Sea Route (CESR) domain were identified to analyse absolute sea level changes (Fig. 1).

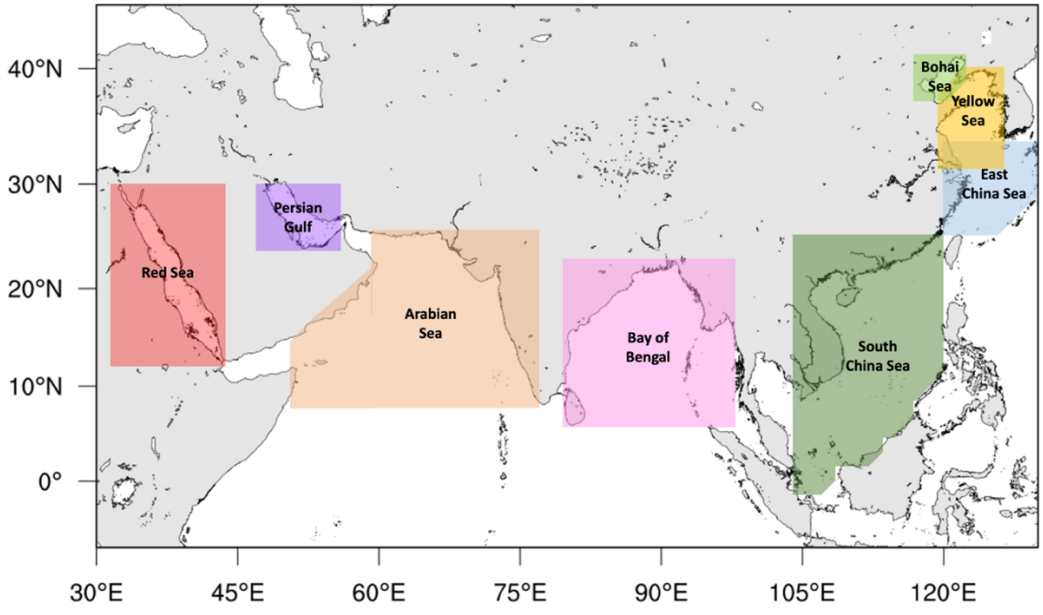

Figure 1: Areas of Interest: Red Sea, Persian Gulf, Arabian Sea, Bay of Bengal, South China Sea, East China Sea, Yellow Sea and Bohai Sea

Figure 2 presents time series (1993–2023) of yearly mean sea level anomalies, averaged over the Global Ocean and the eight CESR sub-basins. The global time series is corrected for Glacial Isostatic Adjustment (GIA) effects using the ICE5G-VM2 GIA model (Peltier, 2004). Linear sea-level trends are calculated for three consecutive 11-year intervals (1993–2003, 2003–2013, and 2013–2023), with each period including an overlapping year to ensure continuity in the analysis and reduce the influence of interannual variability. The associated standard errors are provided in Table 1.

https://doi.org/10.5194/egusphere-2025-1763
Preprint. Discussion started: 10 June 2025
© Author(s) 2025. CC BY 4.0 License.

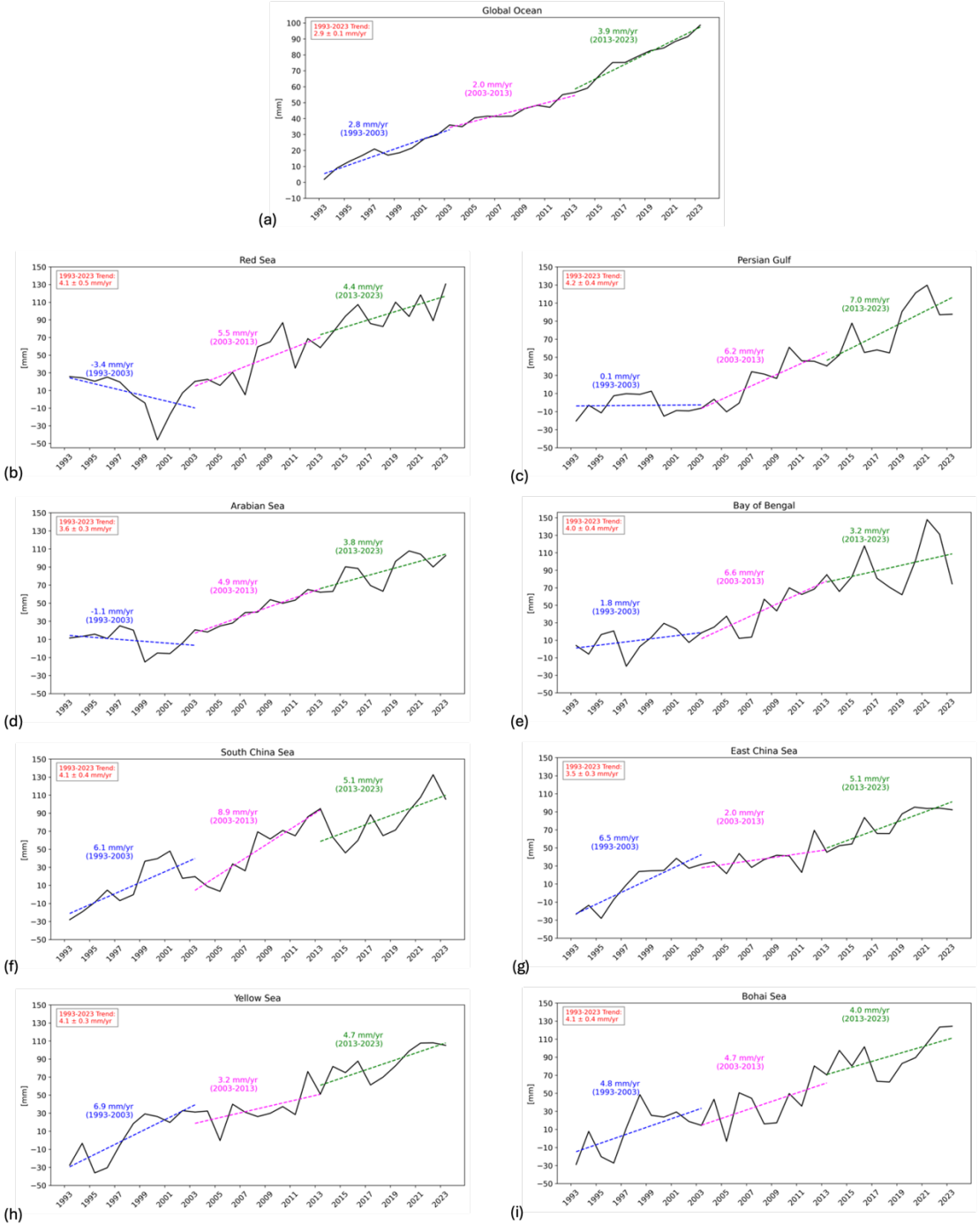

Figure 2: Time series (1993-2023) of monthly means of sea level anomaly (black curve) from altimetry averaged over (a) Global Ocean, (b) Red Sea, (c) Persian Gulf, (d) Arabian Sea, (e) Bay of Bengal, (f) South China Sea, (g) East China Sea, (h) Yellow Sea and (i) Bohai Sea. The coloured dashed lines represent linear sea-level trends over three successive time spans. The product used for the analysis is provided by CMEMS with nomenclature SEALEVEL_GLO_PHY_CLIMATE_L4_MY_008_057.

https://doi.org/10.5194/egusphere-2025-1763
Preprint. Discussion started: 10 June 2025
© Author(s) 2025. CC BY 4.0 License.

Table 1. Sea level anomaly trends obtained from satellite altimetry [mm/yr] covering the areas of interest (Fig. 1) during 1993-2023, 1993-2003, 2003-2013 and 2013-2023 yrs. Bold values indicate significant trends.

Area	1993-2023 [mm/yr]	1993-2003 [mm/yr]	2003-2013 [mm/yr]	2013-2023 [mm/yr]
Global Ocean	**2.9 ± 0.1**	**2.8 ± 0.3**	**2.0 ± 0.2**	**3.9 ± 0.2**
Red Sea	**4.1 ± 0.5**	-3.4 ± 1.9	**5.5 ± 1.9**	**4.4 ± 1.4**
Persian Gulf	**4.2 ± 0.4**	0.1 ± 1.1	**6.2 ± 1.3**	**7.0 ± 2.0**
Arabian Sea	**3.6 ± 0.3**	-1.1 ± 1.2	**4.9 ± 0.4**	**3.8 ± 1.2**
Bay of Bengal	**4.0 ± 0.4**	1.8 ± 1.3	**6.6 ± 1.3**	3.2 ± 2.6
South China Sea	**4.1 ± 0.4**	**6.1 ± 1.5**	**8.9 ± 1.2**	**5.1 ± 1.9**
East China Sea	**3.5 ± 0.3**	**6.5 ± 1.0**	2.0 ± 1.1	**5.1 ± 0.9**
Yellow Sea	**4.1 ± 0.3**	**6.9 ± 1.4**	3.2 ± 1.5	**4.7 ± 1.1**
Bohai Sea	**4.1 ± 0.4**	**4.8 ± 1.9**	**4.7 ± 2.0**	**4.0 ± 1.7**

During the full period (1993 – 2023), SLA trends across the CESR sub-regions are 20 – 45% higher than the global mean trend, with significant spatial and distinct decadal patterns. In the first decade (1993 – 2003), the four Indian Ocean sub-regions exhibit lower trends compared to the global mean, while the four Pacific sub-regions display higher trends. Mean SLA trends increase eastward, from a minimum of -3.4 mm/yr in the Red Sea to a maximum of 6.9 mm/yr in the Yellow Sea, before slightly decreasing in the Bohai Sea (4.8 mm/yr). By the second decade (2003 – 2013), the spatial distribution shifts: regions like the Persian Gulf and Bay of Bengal, previously exhibiting low trends, become areas of maximum SLA trends, while the East China and Yellow Seas experience declining trends. The SLA trend increases significantly in the Red Sea (262%), Persian Gulf (610%), Arabian Sea (545%), Bay of Bengal (267%), and South China Sea (46%), whereas the East China and Yellow Seas exhibit slowdown. In the most recent decade (2013 – 2023), SLA trends decrease in five sub-regions (Red Sea, Arabian Sea, Bay of Bengal, South China Sea, and Bohai Sea) while increasing in the Persian Gulf, East China Sea, and Yellow Sea (Fig. 3).

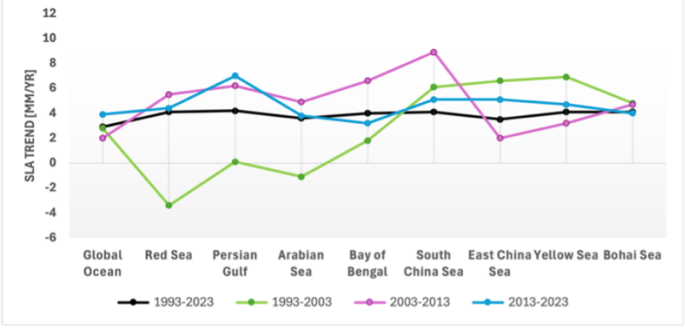

Figure 3. Regional mean sea level trends obtained from satellite altimetry [mm/yr] for the different areas (Fig. 1) during 1993-2023, 1993-2003, 2003-2013 and 2013-2023 periods

https://doi.org/10.5194/egusphere-2025-1763
Preprint. Discussion started: 10 June 2025
© Author(s) 2025. CC BY 4.0 License.

While these trends are indicative of significant decadal variability, not all trends meet the statistical significance threshold (p-value < 0.05). Statistically significant trends, confirm consistent and systematic changes in sea level trends by decade and across regions. Notably the East China Sea, Yellow Sea and Bohai Sea show a decadal trend slowdown in the second (2003-2023) and third decade (2013-2023) with respect to the first one (1993-2003).

The observed decadal variability in SLA trends across the CESR domain arises from complex interactions between natural and anthropogenic factors. Steric changes (thermal expansion and salinity variations) and ocean mass redistribution due to ice melt and terrestrial water storage are primary drivers of global SLA trends (Cazenave and Moreira, 2022). Regional atmospheric and oceanic processes, such as evaporation, precipitation and runoff variability, further influence regional SLA trends. For instance, the mass transport across the lateral boundaries of the regions, due to decadal changes in wind driven circulation, significantly affects SLA trends in specific areas (Cazenave et al., 2014, Borile et al., 2025).

Large-scale climate oscillations, including the El Niño-Southern Oscillation (ENSO), Indian Ocean Dipole (IOD), and North Atlantic Oscillation (NAO), further modulate regional ocean dynamics, contributing to SLA variability (Cazenave & Moreira, 2022). Additionally, localized phenomena, such as monsoonal intensification and basin-scale circulation changes, amplify SLA variability in areas like the Arabian Sea and South China Sea.

Figure 4 illustrates the spatial distribution of SLA trends (mm/yr) for 1993 – 2023, overlaid with climatological surface currents from the Global Multi-Year product (GLOBAL_MULTIYEAR_PHY_001_030) by CMEMS. Minimum SLA trends (2–3 mm/yr) are observed near western boundary currents like the Kuroshio and its branches. In contrast, SLA trends exceed 4 mm/yr along the coasts of the Yellow and East China Seas. The South China Sea displays maximum SLA trends in its open ocean regions, influenced by stronger westward currents through the Luzon Strait compared to southeastern warm currents. Beibu Bay and Vietnam's eastern coastal waters exhibit trends around 4 mm/yr, while the Gulf of Thailand shows lower trends (~3 mm/yr). The highest SLA trend (~5 mm/yr) is found in the eastern Bay of Bengal.

https://doi.org/10.5194/egusphere-2025-1763
Preprint. Discussion started: 10 June 2025
© Author(s) 2025. CC BY 4.0 License.

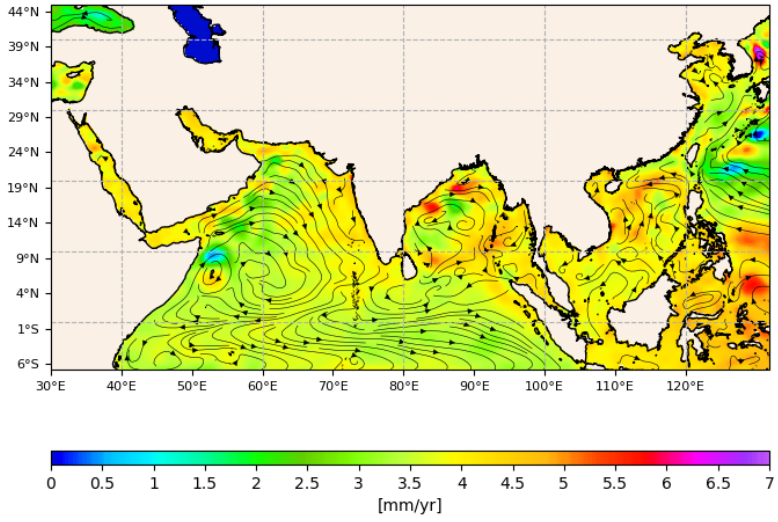

Figure 4. Absolute Sea level trend [mm/yr] computed using the monthly means (seasonal signal removed) over the years 1993-2023 from the CMEMS product SEALEVEL_GLO_PHY_CLIMATE_L4_MY_008_057. Climatological surface currents, obtained from the CMEMS product GLOBAL_MULTIYEAR_PHY_001_030, are superimposed as streamlines.

3.1.2 Relative sea level

Relative sea level is measured at tide gauge stations relative to specific reference levels, such as a multi-year local mean or a standardized national reference level. These measurements capture the ocean surface height relative to the land, incorporating effects like subsidence or bradyseism. Tide gauges, which have been operational since the 18th century, provide localized, long-term insights into sea level dynamics, supporting research on climate change, ocean circulation, extreme events, and coastal hazard assessments. Despite their invaluable role, tide gauge measurements must be integrated with satellite altimetry data to offer a comprehensive view of sea level changes, particularly in regions with complex oceanographic and atmospheric dynamics, such as the China-Europe Sea Route (CESR).

For this study, a subset of tide gauge stations from the Revised Local Reference (RLR) dataset with records starting in 1993 was selected (Fig. 5). Observations from these stations were compared with data from the nearest altimetry grid points.

The comparison of SLA nearest grid point time series with tide gauges data reveal strong correlations (0.9 – 1.0) for most stations, except for Sabang (Bay of Bengal, corr. coef. 0.6) and Masira (Arabian Sea, corr. coef. 0.1). Figure 6 shows the time series for both datasets, highlighting their overall consistency. However, some discrepancies were identified in some stations due to local vertical land movements.

https://doi.org/10.5194/egusphere-2025-1763
Preprint. Discussion started: 10 June 2025
© Author(s) 2025. CC BY 4.0 License.

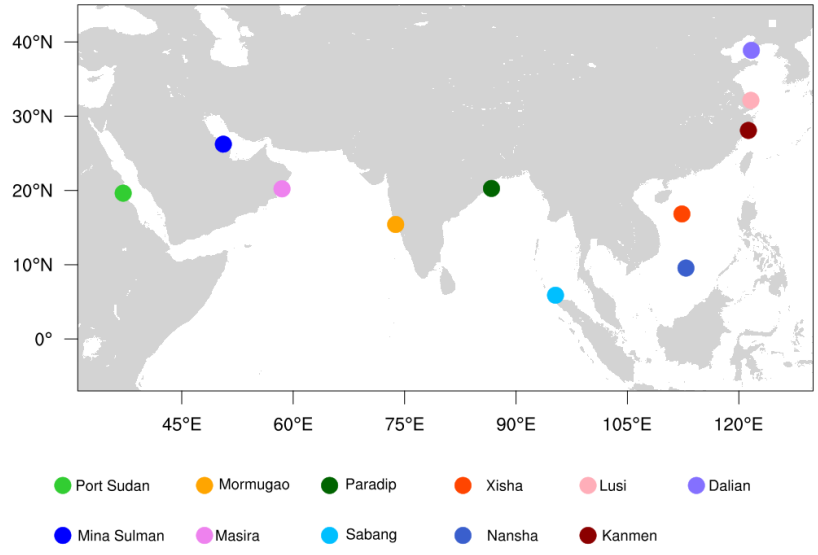

Figure 5. PSMSL tide gauge station's geographical locations

https://doi.org/10.5194/egusphere-2025-1763
Preprint. Discussion started: 10 June 2025
© Author(s) 2025. CC BY 4.0 License.

Figure 6. Time series (1993-2023) of monthly means of sea level anomaly (mm) at the platforms: (a) Port Sudan (Red Sea) , (b) Mina Sulman (Persian Gulf), (c) Mormugao (Arabian Sea), (d) Masira (Arabian Sea), (e) Paradip (Bay of Bengal), (f) Sabang (Bay of Bengal), (g) Xisha (South China Sea), (h) Nansha (South China Sea), (i) Kanmen (East China Sea), (l) Lusi (Yellow Sea), and (m) Dalian (Bohai Sea). Tide gauge stations observations are reported in blue and altimetry data overlaid in orange at each station.

https://doi.org/10.5194/egusphere-2025-1763
Preprint. Discussion started: 10 June 2025
© Author(s) 2025. CC BY 4.0 License.

Table 2 provides a detailed comparison of sea level trends and associated uncertainties (expressed as standard errors) for each selected PSMSL station using both in-situ and satellite data over multiple periods: 1993–2022, 1993–2002, 2003–2012, and 2013–2022. Altimetric trends were computed at the grid point nearest to the tide gauge stations, while in-situ trends were excluded where yearly observations were less than 70% of the expected data for the reference period. Notably, 2023 data were omitted from the analysis, as only the Paradip station (Bay of Bengal) reported observations for that year. Bold p-values in Table 2 indicate statistically significant trends, emphasizing the reliability of those results.

Table 2. Sea level trends with standard errors (p-values in parentheses) calculated for each selected PSMSL station using in-situ and satellite data over the periods 1993–2022, 1993–2002, 2003–2012, and 2013–2022. 2023 is not considered since tide gauge is only available for the Paradip station (Bay of Bengal). Altimetric trends were computed at the grid point nearest to the tide gauge, while in-situ trends were excluded (NA) where yearly observations were <70% of the expected data for the reference period. Bold indicate statistically significant trends.

Station name (PSMSL)	Trend 1993-2022 [mm/yr]		Trend 1993-2002 [mm/yr]		Trend 2003-2012 [mm/yr]		Trend 2013-2022 [mm/yr]	
	In-situ	*Satellite*	*In-situ*	*Satellite*	*In-situ*	*Satellite*	*In-situ*	*Satellite*
Port Sudan (Red Sea)	NA	**4.0 ± 0.6**	NA	**-7.2 ± 1.7**	NA	**5.9 ± 2.3**	NA	3.9 ± 2.0
Mina Sulman (Persian Gulf)	NA	**4.4 ± 0.5**	NA	-0.6 ± 1.6	NA	**7.6 ± 1.4**	NA	**8.0 ± 2.8**
Mormugao (Arabian Sea)	**8.6 ± 1.0**	**4.5 ± 0.4**	NA	-1.3 ± 1.5	**8.7 ± 3.2**	**5.8 ± 1.3**	**14.9 ± 3.9**	**6.8 ± 2.6**
Masira (Arabian Sea)	NA	**4.1 ± 0.4**	NA	-1.4 ± 1.5	NA	**4.8 ± 2.0**	NA	3.4 ± 1.7
Paradip (Bay of Bengal)	NA	**4.6 ± 0.7**	NA	6.2 ± 4.4	**9.9 ± 3.9**	**7.4 ± 1.7**	7.5 ± 7.0	7.9 ± 4.6
Sabang (Bay of Bengal)	NA	**4.1 ± 0.7**	NA	4.3 ± 4.2	NA	**7.6 ± 2.7**	NA	3.6 ± 4.1
Xisha (South China Sea)	**5.0 ± 1.0**	**4.7 ± 0.8**	6.5 ± 4.4	**8.7 ± 3.5**	10.8 ± 5.9	7.4 ± 5.4	2.6 ± 4.7	0.1 ± 3.4
Nansha (South China Sea)	NA	**3.6 ± 0.5**	NA	**8.4 ± 2.2**	**15.8 ± 2.4**	**10.0 ± 2.3**	NA	4.0 ± 2.1
Kanmen (East China Sea)	**5.2 ± 0.6**	**3.5 ± 0.5**	4.8 ± 2.6	**9.2 ± 1.7**	**8.7 ± 2.4**	2.5 ± 2.0	1.3 ± 3.3	1.3 ± 2.8

https://doi.org/10.5194/egusphere-2025-1763
Preprint. Discussion started: 10 June 2025
© Author(s) 2025. CC BY 4.0 License.

Lusi (Yellow Sea)	NA	**4.6 ± 0.5**	NA	**10.9 ± 2.4**	9.2 ± 3.7	1.8 ± 2.8	-0.1 ± 5.9	5.6 ± 2.8
Dalian (Bohai Sea)	**4.4 ± 0.4**	**4.7 ± 0.3**	**7.8 ± 2.0**	**7.5 ± 1.8**	2.1 ± 1.9 (0.30)	2.4 ± 1.7 (0.20)	**4.8 ± 1.9**	**8.2 ± 1.3**

For the tide gauge stations data, sea level rise trend results at stations Port Sudan (Red Sea), Mina Sulman (Persian Gulf), Masira (Arabian Sea) and Sabang (Bay of Bengal) are not available as the data interval gaps are too large. High relative sea level rise trends (4.4–8.6 mm/yr) were observed at stations such as Mormugao (Arabian Sea), Xisha (South China Sea), Kanmen (East China Sea), and Dalian (Bohai Sea). For most stations, trends derived from satellite altimetry and tide gauges were consistent within error bounds.

The difference of Lusi in the Yellow Sea and Kanmen in the East China sea are most likely caused by the land subsidence (Xue et al., 2005; Zhu et al., 2015). In the Indian Ocean, earthquakes can cause large land vertical movement, for example, the 2007 Bengkulu earthquake also caused significant vertical displacements of up to 0.8 m in a wider area of Sumatra measured directly with GPS and confirmed by modelling (Borrero et al. 2009). Fenoglio-Marc et al. (2012) studied the sea level trend in the Indonesian region and found that the observations from tide gauges are affected by vertical land movements due to the seismic displacements. The consistency between satellite and tide gauge data can be improved applying GPS corrections but these data are not available in the PSMSL database.

These results demonstrate substantial spatial and decadal variability in relative sea level trends across the CESR region, driven by factors such as vertical land motion, steric effects, and regional circulation dynamics.

3.1 Extreme sea level events

During a severe storm, water levels at the coast will rise as a result of atmospheric pressure changes and the winds (Pugh & Woodworth, 2015). This causes storm surges, resulting in water levels that can be up to several meters above Mean Sea Level (MSL), especially when coinciding with high tide. In addition, there might also be coastally trapped non-isostatic signals from large scale pressure patterns that could amplify the local wind and tidal effects (Zhao et al., 2017, Park et al., 2021).

The CESR region is indeed prone to extreme sea levels, and several factors contribute to this vulnerability, among others tropical and extratropical cyclones. It is reported that in the Red Sea, the extreme sea level in the basin is about 0.30-0.50 m, and the extreme sea level in the Gulf of Suez is about 0.85 m (Antony et al., 2022). In the Persian Gulf, the probability of storm surges is low. However, Lin and Emanuel (2016) have shown that tropical cyclones could occur in that region causing surges of up to 4 m in Dubai, but with a return period more than 10,000 years. The Bay of Bengal is an area particularly prone to high extreme sea levels (Dube et al., 2009; Lewis et al, 2013), experiencing, on average, five surge events per decade exceeding a surge level of 5m (Needham et al., 2015). Regions in North-western Pacific, including China and the Philippines, can experience tropical cyclones and high storm surges (Zhang et al., 2015; Fang et al., 2021). For example, the once-in-50-

https://doi.org/10.5194/egusphere-2025-1763
Preprint. Discussion started: 10 June 2025
© Author(s) 2025. CC BY 4.0 License.

years extreme sea levels along the coastline of China from the south of Shandong Peninsula to the Beibu Gulf, range between 1.6 m and 3.2 m (Zhang & Sheng, 2015).

The analysis of the extreme sea levels is done using both the Hawaii tide gauge stations and the GTSMip and COAST-RP model data sets (the model validation is shown in Appendix A). A common approach for quantification of extremes is based on Extreme Value Analysis (EVA), expressing the probability of exceedance for various water levels, for example the 1 in 100-year return period. This is achieved by fitting an extreme value distribution to extremes, for example Gumbel or Generalized Pareto Distribution. Extremes can be either extracted from high-frequency time-series using block maxima, such as monthly or annual maxima, or by using a peak value over a certain threshold, such as the 99th percentiles or r-largest (Arns et al., 2013; Wahl et al., 2017).

Figure 7 maps the Mean Highest High Water (MHHW) and Highest Astronomical Tide (HAT), which show values exceeding 2 m in the Gulf of Khambhat (India), Andaman Sea bordering Myanmar, west of North and South Korean, and along the coastline of China in the East China Sea between Shandong and Fujian province.

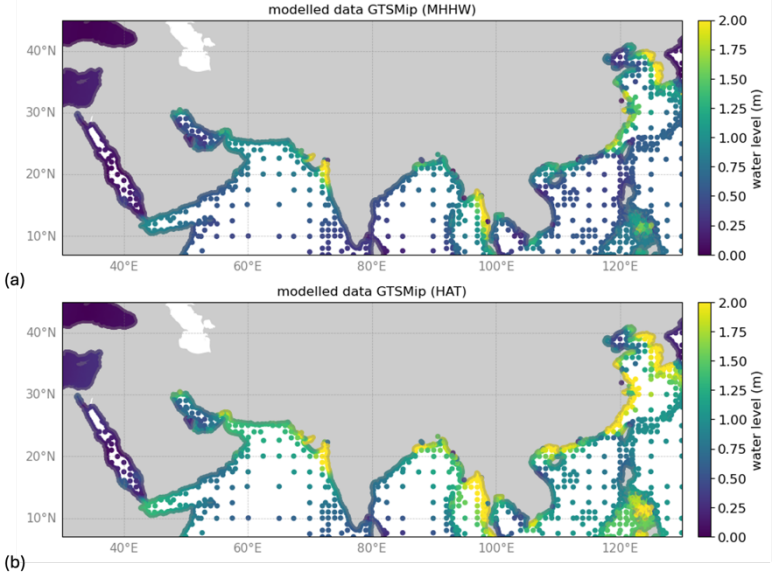

Figure 7. Overview of the tidal levels in the region over the period 1985-2014 derived from the GTSMip dataset. (Top) Mean Higher High Water (MHHW) (Bottom) Highest Astronomical Tide (HAT)

Figure 8 shows that the return period levels of extreme sea level at several selected tide gauge stations are generally consistent, especially for lower return periods, but there are also relevant differences. For Zhapo, Hong Kong and Shanwei the observations show overlap with the modelled data. For higher return periods, the deviations are somewhat higher, but this is likely caused by differences in the length of timeseries. For Zhapo there are tropical cyclones that can cause much higher water levels than measured in the observational record. Also, for Hong Kong and Shanwei, the values of COAST-RP are higher than GTSMip, with larger deviations for higher return periods. This indicates the need for the use of synthetic tropical cyclones to

https://doi.org/10.5194/egusphere-2025-1763
Preprint. Discussion started: 10 June 2025
© Author(s) 2025. CC BY 4.0 License.

get the relevant extreme sea levels in all stations. For Xiamen the results show that while the slope of the extreme value distribution of the modelled data agrees with the observations, there is an offset of about 0.3 m with observations. Efforts are underway to try to harmonize the datum by removing the annual means, since this is potentially the reason for the discrepancy in the vertical datum. It could also be that there is a strong seasonal component in mean sea level driven by a process that is not resolved by GTSM. GTSM is a depth-averaged barotropic model and does not simulate density-driven processes nor include river inflows.

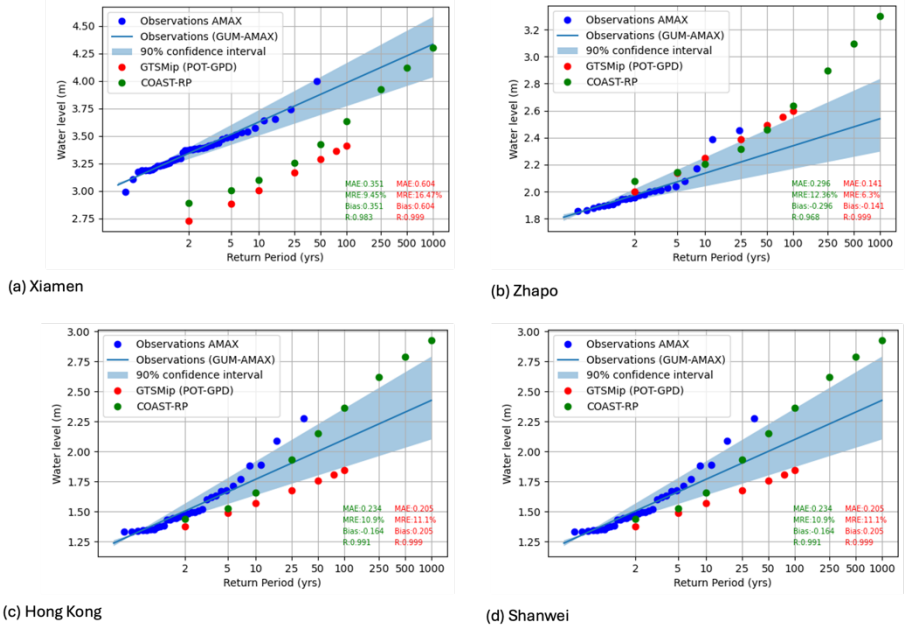

Figure 8. Extreme value plot for selected stations showing observations in blue (annual maxima in dots, line shows Gumbel fit, and 90% confidence interval based on bootstrapping in shaded area), GTSMip in red, and COAST-RP in green

4 Conclusions and discussions

This study provides a detailed analysis of sea level trends, and extreme events across the China-Europe Sea Route (CESR) region at decadal and multidecadal time scales, leveraging both global and regional datasets, including satellite altimetry and tide gauge measurements. The findings highlight the complexity of sea level change in this region, which are driven by a combination of natural variability, anthropogenic influences, and localized dynamics. These insights have significant implications for regional risk assessment and coastal adaptation strategies.

The observed mean sea level regional trends exhibit notable spatial and decadal variability, emphasizing the importance of a multi-decadal perspective. Over the 1993–2023 period, mean sea level trends across CESR sub-regions were 20–45% higher than the global mean trend for the multidecadal period, 1993-2023, with considerable eastward increases. Notably decadal

https://doi.org/10.5194/egusphere-2025-1763
Preprint. Discussion started: 10 June 2025
© Author(s) 2025. CC BY 4.0 License.

showdowns in the East China Sea, Yellow Sea and Bohai Bay mean sea level are present probably connected to the interplay of circulation changes affecting the mass transport across the open ocean boundaries, the water cycle and the steric sea level. This analysis confirms that absolute sea level trends in the CESR have experienced significant positive acceleration in North Indian Ocean. This is significantly higher than the global sea level rise trends driven by climate change. However, in the Pacific side (South and East China Sea) there is a slowdown that could be due to interannual climate variability of the local water cycle, the circulation and the steric effects as described for the global ocean by Cazenave et al. (2012) and Borile et al. (2025) for the Mediterranean Sea.

The reasons for decadal variability of SLA trend across sub-regions should be further investigated. Huang et al. (2023) found that Tropical SW Indian Ocean SLA exhibits a distinct multidecadal sea-level falling trend from the 1960s to the early 2000s. However, the trend shifts to a strong rising trend of 4.05 ± 0.56 cm/decade. This is like what we found in CESR sub-regions North Indian Ocean. He also found that atmospheric circulation over the South Indian Ocean shifted from a cyclonic pattern during 1960–1999 to an anticyclonic pattern during 2002–2021. Huang's budget analysis finds that SLA rise of 1. 20 ± 0.20 cm/decade in the upper 2,000 m can be attributed to the Ekman pumping and deep-water warming, which accounting for 30% of the total sea level rise. We expect that similar reasons may contribute to the observed SLA trend acceleration in the North Indian Ocean. In the Pacific side of the CESR, the mass and steric components of the mean sea level trends compose to give a second decade (2003-2013) trend decrease probably connected to water cycle displacements, as found already for the global mean sea level trend (Cazenave et al., 2012).

The integration of tide gauge and altimetry data was critical in validating sea level trends. The results revealed discrepancies in satellite mean sea level trends and tide gauges in specific locations. We argue that these discrepancies could be primarily due to factors such as land subsidence, seismic activity, and limitations in coastal altimetry products.

The study investigated extreme sea level events, revealing significant regional differences in return periods and magnitudes. For instance, the Bay of Bengal and the northwestern Pacific are particularly prone to high extreme sea levels, driven by tropical cyclones and storm surges. The results demonstrated that while existing hydrodynamic models like GTSM capture general patterns, discrepancies persist due to model limitations, such as the underestimation of winds in ERA5 reanalysis data and the absence of density-driven processes in the GTSM. Synthetic cyclone tracks, as employed in the COAST-RP dataset, proved essential for refining extreme sea level estimates, particularly for higher return periods.

The return periods presented in this study could be used in combination with flood and impact models to estimate the population that could potentially be exposed to coastal flooding or the computed flood risk (i.e., expected annual damages). Moreover, the data could be combined with sea-level rise and climate projections to evaluate how extreme sea levels and coastal flood risk may change under future climate conditions.

In conclusion, this study underscores the importance of regional analysis to capture the complex drivers of sea level changes in the CESR region. The results highlight significant spatial and temporal variability in SLA trends across the CESR region, driven by a complex interplay of regional processes due to water balance and regional circulation. Higher resolution, region-specific datasets and models are essential for disentangling natural variability from anthropogenic forcing and they should be

https://doi.org/10.5194/egusphere-2025-1763
Preprint. Discussion started: 10 June 2025
© Author(s) 2025. CC BY 4.0 License.

used in future work. Such advancements are vital for enhancing coastal resilience, informing navigation strategies, and supporting adaptation planning in this economically and geopolitically significant region.

Appendix A: model validation

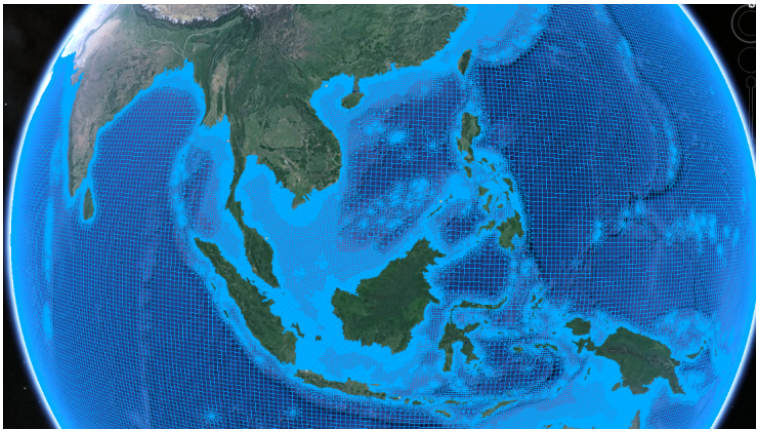

Figure A1: Grid of the Global Tide and Surge Model for Southeast Asia. See more https://publicwiki.deltares.nl/display/GTSM/Model+description+and+development

To validate the return periods extracted from GTSM, hourly observations from tide gauge stations are used. In this case, observations are retrieved from the University of Hawaii Sea Level Center Dataset (UHSLC, https://uhslc.soest.hawaii.edu/datainfo/). There are 52 tide gauge stations in the area of interest (between 7-45° North and 30-130° East). The total number of records found numbers '15', because of using only the tide gauge stations with a minimum record of 25 years and a maximum of 20% of missing data. If we use all stations that have more than 10 years of data, this increases to 36 stations (Figure A2). For each station, the annual mean is removed to reference all data to the same vertical datum. Extreme value analysis is used to estimate the water levels corresponding to different return periods. Specifically, a Generalized Pareto Distribution is fitted to the peaks above a threshold, defined as the 99th percentile. The independence of the peaks is ensured by assuming a minimum of 72h between peaks. The GPD is parameterized by shape, location, and scale parameters obtained here following Maximum Likelihood Estimation (MLE). The starting estimate for the fit of the shape parameter is set to 0 to minimize the effect of outliers.

https://doi.org/10.5194/egusphere-2025-1763
Preprint. Discussion started: 10 June 2025
© Author(s) 2025. CC BY 4.0 License.

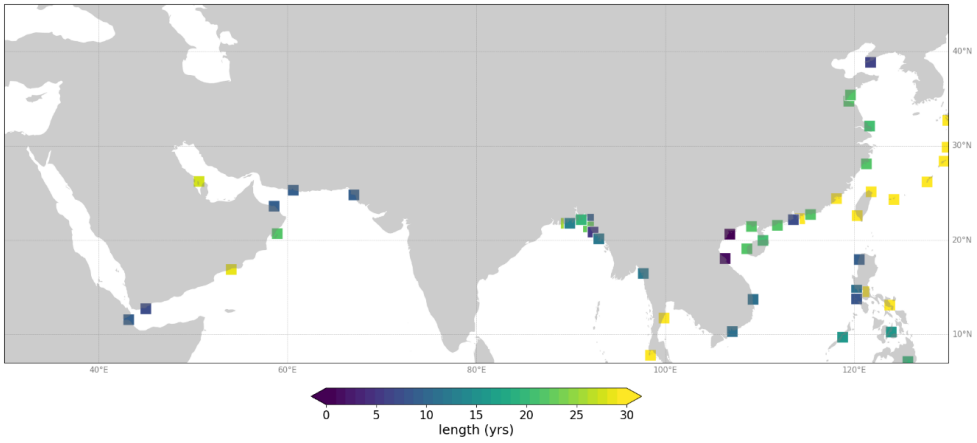

Figure A2: Map of available tide gauge stations of the UHSLC dataset and their corresponding record length (years). From the available tide gauge stations, only stations with more than 25 years of data were used for the validation in this study.

The upper panel in Figure A3 shows the return periods for the tide gauge stations. It shows that the 100-year high water level events reach 3 m in the mouth of the Bay of Bengal, along the western coast of the Yellow, East and South China Seas. Lower values are seen for the stations in the other regions. A comparison between the return periods computed for the tide gauge stations and the GTSM model shows that the overall performance is good. The correlation coefficients of the return periods from the tidal gauge stations (using POT and fitting Gumbel distribution to the annual maxima) and GTSM model values against their respective water levels yielded a correlation coefficient of 0.96 and >0.99. The mean bias (MB) is 0.10 m for COAST-RP and 0.14 m for GTSMip. The mean absolute error (MAE) is 0.37 (S.D. 0.33) for COAST-RP and 0.33 (S.D. 0.34) for GTSMip. It shows that, on average, for the 1 in 100-year return level the datasets are comparable in performance. The middle and bottom panels in Figure 8 show a comparison of the observed return levels with modelled return levels from, respectively, GTSMip and COAST-RP. It shows that the water level is underestimated at most locations, but that for many stations, the errors are smaller than 0.5 m. Errors could be larger in regions prone to tropical cyclones, such as the Philippines. In these regions, a single event in the observations can heavily influence the return period estimations. On the one hand, those extremes will likely be underestimated in the GTSMip dataset which is based on the ERA5 climate reanalysis forcing.

The difference between GTSMip (upper panel) and COAST-RP (middle panel) in Figure A4 reflects the larger sample for tropical cyclones and differences in the extreme value analysis. With a value exceeding 0.5 m, the differences between the two datasets are relatively large. GTSMip mostly shows an underestimate compared to COAST-RP, with the largest difference in the Philippines, Cambodia and near South Korea, but there are also regions of over-estimates such as the Pacific Kuril Islands. The probabilities in COAST-RP are more robust than for GTSMip and the COAST-RP is expected to perform better in regions prone to tropical cyclones. Basically, the 40 years of ERA5 simulations are too short to estimate tropical cyclone probabilities. In other regions, the differences are much smaller (e.g., Red Sea region) and are mainly caused by a difference in the methodology used for the extreme value analysis.

https://doi.org/10.5194/egusphere-2025-1763
Preprint. Discussion started: 10 June 2025
© Author(s) 2025. CC BY 4.0 License.

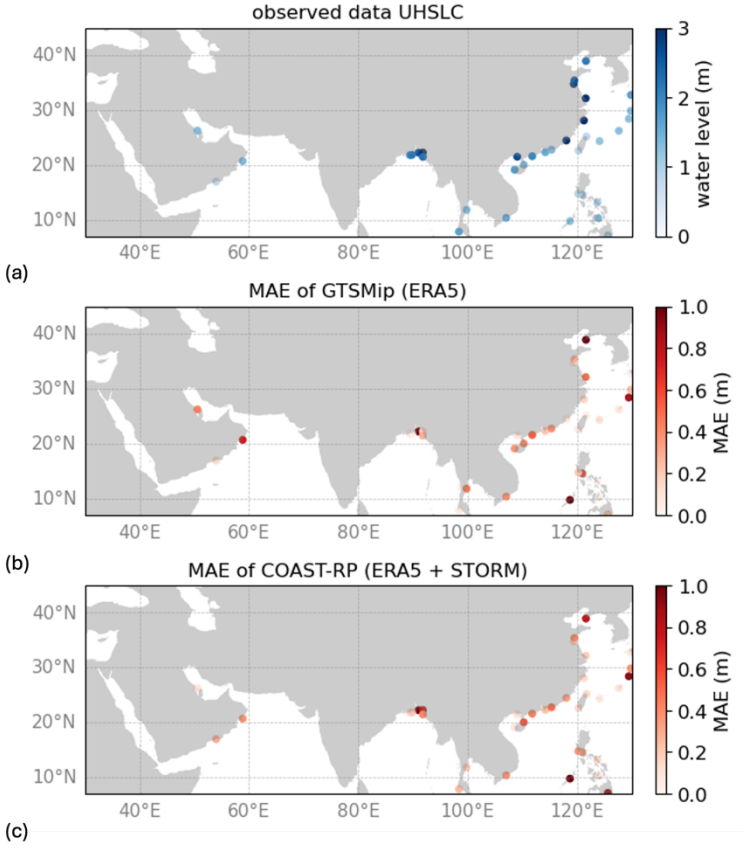

Figure A3: Full dataset of observed and modelled water levels corresponding to a return period of 100-years. The top panel shows the observed water levels from UHSLC. The middle and the lower panels show the Mean Absolute Error (MAE) for GTSMip and COAST-RP respectively.

https://doi.org/10.5194/egusphere-2025-1763
Preprint. Discussion started: 10 June 2025
© Author(s) 2025. CC BY 4.0 License.

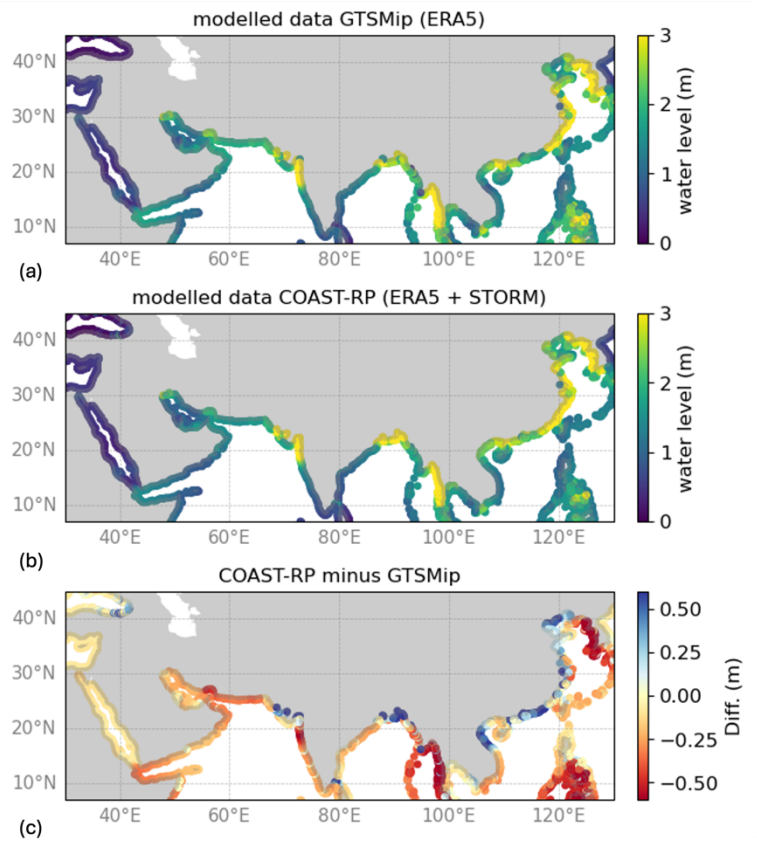

Figure A4: Overview of 1 in 100-year exceedance events for extreme surges. (Top) Extreme surge levels from GTSMip forced with ERA5. (Middle) Extreme surge levels from Coast-RP. (Bottom) Difference between GTSMip and Coast-RP surge levels. Return levels are below 1 m for most of the coastline of the Red Sea (e.g., Egypt, Sudan, Yemen, eastern Saudi Arabia). Values between 1 and 2 m are seen for most of the Persian Gulf (e.g., Iran, Oman, and eastern Saudi Arabia), Arabian Sea (e.g., Pakistan), southwest coast of the Bengal Bay (India) and parts of the South China Sea (e.g., Vietnam). Regions where the 1 in 100-year water levels exceed 2 m includes northern part of Bay of Bengal (Bangladesh), north-eastern part of the Arabian Sea (west India and southeast Pakistan), Gulf of Thailand (Cambodia) and the Yellow Sea (northern China).

Author contribution:

RL and RG wrote the manuscript with contributions from all co-authors. RL, RG, KY and SaM performed the data analysis. NP, JS, SiM, MV and EK critically reviewed the paper and contributed to data interpretation. JBC coordinated the project. All authors reviewed and approved the final version of the manuscript.

https://doi.org/10.5194/egusphere-2025-1763
Preprint. Discussion started: 10 June 2025
© Author(s) 2025. CC BY 4.0 License.

Acknowledgements

Part of the data and information obtained, and work implemented leading to this publication was possible thanks to the financial support from the European Union under the EC-PI funded project EuropeAid/139904/DH/SER/CN - 410737 Partnership Instrument EMOD-PACE (EMODnet PArtnership for China and Europe). R.G. is supported by a National University of Singapore Graduate Research Scholarship.

Competing interests: The authors declare that they have no conflict of interest.

References

Alam, E., and Dominey-Howes, D.: A new catalogue of tropical cyclones of the northern Bay of Bengal and the distribution and effects of selected landfalling events in Bangladesh, International Journal of Climatology, 35, 801–835, https://doi.org/10.1002/joc.4035, 2014.

Ali, A.: Climate change impacts and adaptation assessment in Bangladesh, Climate Research, 12, 109–116, https://doi.org/10.3354/cr012109, 1999.

Antony, C., and Unnikrishnan, A.: Observed characteristics of tide-surge interaction along the east coast of India and the head of Bay of Bengal, Estuarine, Coastal and Shelf Science, 131, 6–11, https://doi.org/10.1016/j.ecss.2013.08.004, 2013.

Antony, C., Langodan, S., Dasari, H. P., Abualnaja, Y., and Hoteit, I.: Sea-level extremes of meteorological origin in the Red Sea. Weather and Climate Extremes, 100409, 2022.

Arns, A., Wahl, T., Haigh, I., Jensen, J., and Pattiaratchi, C.: Estimating extreme water level probabilities: A comparison of the direct methods and recommendations for best practice. Coastal Engineering, 81, 51-66, 2013.

Baburaj, P. P., Abhilash, S., Mohankumar, K., and Sahai, A. K.: On the Epochal Variability in the Frequency of Cyclones during the Pre-Onset and Onset Phases of the Monsoon over the North Indian Ocean. Adv. Atmos. Sci. 37, 634–651. doi:10.1007/s00376-020-9070-5, 2020.

Balaguru, K., Foltz, G. R., and Leung, L. R.: Increasing Magnitude of Hurricane Rapid Intensification in the Central and Eastern Tropical Atlantic. Geophys. Res. Lett. 45, 4238–4247. doi:10.1029/2018GL077597, 2018.

Bhatia, K., Vecchi, G., Murakami, H., Underwood, S., and Kossin, J.: Projected response of tropical cyclone intensity and intensification in a global climate model. J. Clim. 31, 8281–8303. doi:10.1175/JCLI-D-17-0898, 2018.

Bloemendaal, N., de Moel, H., Muis, S., Haigh, I. D., and Aerts, J. C. J. H.: Estimation of global tropical cyclone wind speed probabilities using the STORM dataset. Scientific Data, 7, 1-11. [377]. https://doi.org/10.1038/s41597-020-00720-x, 2020.

Borile, F., Pinardi, N., Lyubartsev, V., Ghani, M. H., Navarra, A., Alessandri, J., Clementi, E., Coppini, G., Mentaschi, L., Verri, G., da Costa, V. S., Scoccimarro, E., Misurale, F., Novellino, A., & Oddo, P.: The Eastern Mediterranean Sea mean sea

https://doi.org/10.5194/egusphere-2025-1763
Preprint. Discussion started: 10 June 2025
© Author(s) 2025. CC BY 4.0 License.

level decadal slowdown: the effects of the water budget. Frontiers in Climate, 7, Article 1472731. https://doi.org/10.3389/fclim.2025.1472731, 2025.

Borrero, J. C., R. Weiss, E.A. Okal, R. Hidayat, Suranto, D. Arcas, and V. V. Titov.: The tsunami of 2007 September 12, Bengkulu province, Sumatra, Indonesia: Post-tsunami field survey and numerical modelling. Geophys. J. Int. 178(1): 180–194. doi:10.1111/j.1365-246X.2008.04058.x, 2009.

Bruneau, N. et al.: Estimation of global coastal sea level extremes using neural networks Environmental Research Letters, 15(7), p. 074030. Available at: https://doi.org/10.1088/1748-9326/ab89d6, 2020.

Calafat, F. M., and Marcos, M.: Probabilistic reanalysis of storm surge extremes in Europe Proceedings of the National Academy of Sciences, 117(4), pp. 1877–1883. Available at: https://doi.org/10.1073/pnas.1913049117, 2020.

Carrère, L., and Lyard, F.: Modeling the barotropic response of the global ocean to atmospheric wind and pressure forcing - comparisons with observations, Geophys. Res. Lett., 30, 1275, doi:10.1029/2002GL016473, 6, 2003.

Cazenave, A., Dieng, HB., Meyssignac, B. et al.: The rate of sea-level rise. Nature Clim Change 4, 358–361, https://doi.org/10.1038/nclimate2159, 2014.

Cazenave A, Moreira L.: Contemporary sea-level changes from global to local scales: a review. Proc. R. Soc. A 478: 20220049. https://doi.org/10.1098/rspa.2022.0049, 2022.

Copernicus: Ocean state report, issue 6. Journal of Operational Oceanography. 15:1–220, 2022.

Copernicus Climate Change Service, Climate Data Store: Sea level gridded data from satellite observations for the global ocean from 1993 to present. Copernicus Climate Change Service (C3S) Climate Data Store (CDS). DOI: 10.24381/cds.4c328c78, 2018.

Dangendorf, S., Frederikse, T., Chafik, L. et al.: Data-driven reconstruction reveals large-scale ocean circulation control on coastal sea level. Nat. Clim. Chang. 11, 514–520. https://doi.org/10.1038/s41558-021-01046-1, 2021.

Dube, S. K., Jain, I., Rao, A. D., and Murty, T. S.: Storm surge modelling for the Bay of Bengal and Arabian Sea. Natural Hazards, 51, 3-27, 2009.

Dullaart, J. C. M., Muis, S., Bloemendaal, N., and Aerts, J. C. J. H.: Advancing global storm surge modelling using the new ERA5 climate reanalysis. Climate Dynamics, 54(1-2), 1007-1021. https://doi.org/10.1007/s00382-019-05044-0, 2020.

Dullaart, J. C. M., Muis, S., Bloemendaal, N., Chertova, M. V., Couasnon, A., and Aerts, J. C. J. H.: Accounting for tropical cyclones more than doubles the global population exposed to low-probability coastal flooding. Communications Earth and Environment, 2, 1-11. [135]. https://doi.org/10.1038/s43247-021-00204-9, 2021.

Ezer, T., Atkinson, L. P., Corlett, W. B. and Blanco, J. L.: Gulf Stream's induced sea level rise and variability along the U.S. mid-Atlantic coast, J. Geophys. Res. Oceans, 118, 685– 697, doi:10.1002/jgrc.20091, 2013.

https://doi.org/10.5194/egusphere-2025-1763
Preprint. Discussion started: 10 June 2025
© Author(s) 2025. CC BY 4.0 License.

Fang, Q., Liu, J., Hong, R., Guo, A., and Li, H.: Experimental investigation of focused wave action on coastal bridges with box girder. Coastal Engineering, 165, 103857, 2021.

Fenoglio-Marc L., T. Schöne, J. Illigner, M. Becker, P. Manurung, and Khafid.: Sea Level Change and Vertical Motion from Satellite Altimetry, tide gauge stations and GPS in the Indonesian Region, Marine Geodesy, 35:sup1, 137-150, 2012.

Fox-Kemper, B., H. T. Hewitt, C. Xiao, G. et al.: Ocean, Cryosphere and Sea Level Change. In: Climate Change 2021: The Physical Science Basis. Contribution of Working Group I to the Sixth Assessment Report of the Intergovernmental Panel on Climate Change. Cambridge University Press. 2021

Hersbach H, Bell B, Berrisford P, et al.: The ERA5 global reanalysis. Q J R Meteorol Soc. 2020; 146: 1999–2049. https://doi.org/10.1002/qj.3803, 2020.

Huang, L., Zhuang, W., Lu, W., Zhang, Y., Edwing, D., & Yan, X.-H.: Rapid sea level rise in the tropical Southwest Indian Ocean in the recent two decades. Geophysical Research Letters, 51, e2023GL106011. https://doi. org/10.1029/2023GL106011, 2024.

IPCC: Climate Change 2021: The Physical Science Basis. Contribution of Working Group I to the Sixth Assessment Report of the Intergovernmental Panel on Climate Change [Masson-Delmotte, V., P. Zhai, A. Pirani, S.L. Connors, C. Péan, S. Berger, N. Caud, Y. Chen, L. Goldfarb, M.I. Gomis, M. Huang, K. Leitzell, E. Lonnoy, J.B.R. Matthews, T.K. Maycock, T. Waterfield, O. Yelekçi, R. Yu, and B. Zhou (eds.)]. Cambridge University Press, Cambridge, United Kingdom and New York, NY, USA, 2391 pp. doi:10.1017/9781009157896, 2021.

Khan MJU, F Durand, K Emanuel, Y Krien, L Testut, and AKMS Islam.: Storm surge hazard over Bengal delta: A probabilistic-deterministic modelling approach. Natural Hazards & Earth System Sciences, 22(7), p2359-2379, 2022.

Kishtawal, C. M., Jaiswal, N., Singh, R., and Niyogi, D.: Tropical cyclone intensification trends during satellite era (1986-2010). Geophys. Res. Lett. 39, 1–6. doi:10.1029/2012GL051700, 2012.

Kossin, J. P., Knapp, K. R., Olander, T. L., and Velden, C. S.: Global increase in major tropical cyclone exceedance probability over the past four decades. Proc. Natl. Acad. Sci. 117, 11975–11980. doi:10.1073/pnas.1920849117, 2020.

Lewis, M., Bates, P., Horsburgh, K., Neal, J., and Schumann, G.: A storm surge inundation model of the northern Bay of Bengal using publicly available data. Quarterly Journal of the Royal Meteorological Society, 139(671), 358-369, 2013.

Lievin, M., Kocha, C., Courcol, B., Philipps, S., Denis, I., Guinle, T., et al. : Reprocessing of Sea Level L2P Products for 28 Years of Altimetry Missions. OSTST. Available online at: meetings.aviso.altimetry.fr/fileadmin//user_upload/tx_ausyclsseminar/files/OS, 2020.

Lin, N., Emanuel, K.: Grey swan tropical cyclones. Nature Clim Change 6, 106–111. https://doi-org.vu-nl.idm.oclc.org/10.1038/nclimate2777, 2016.

Ministry of Natural Resources of the People's Republic of China (MNR) (2023). China Sea Level Bulletin 2022

https://doi.org/10.5194/egusphere-2025-1763
Preprint. Discussion started: 10 June 2025
© Author(s) 2025. CC BY 4.0 License.

Muis, S., Verlaan, M., Winsemius, H. C., Aerts, J. C. J. H., and Ward, P. J.: A global reanalysis of storm surges and extreme sea levels. Nat. Commun. 7:11969. doi: 10.1038/ncomms11969, 2016.

Muis, S., Apecechea, M. I., Dullaart, J., de Lima Rego, J., Madsen, K. S., Su, J., Yan, K., and Verlaan, M.: A High-Resolution Global Dataset of Extreme Sea Levels, Tides, and Storm Surges, Including Future Projections. Frontiers in Marine Science, 7, 1-15. [263]. https://doi.org/10.3389/fmars.2020.00263, 2020.

Muis, S., Aerts, J.C.J.H., Á. Antolínez, J.A., Dullaart, J., Duong, T.M., Erikson, L., Haarmsa, R., Apecechea, M.I., Mengel, M., Le Bars, D., O'Neill, A., Ranasinghe, R., Roberts, M., Verlaan, M., Ward, P.J., Yan, K.: Global projections of storm surges using high-resolution CMIP6 climate models. Earth's Future, 11, e2023EF003479. https://doi.org/10.1029/2023EF003479, 2023.

Needham, H. F., Keim, B. D., and Sathiaraj, D.: A review of tropical cyclone-generated storm surges: Global data sources, observations, and impacts, Reviews of Geophysics, 53, 545–591, https://doi.org/10.1002/2014rg000477, 2015.

Nerem, R.S., B.D. Beckley, J.T. Fasullo, B.D. Hamlington, D. Masters, G.T. Mitchum.: Climate-change–driven accelerated sea-level rise detected in the altimeter era. Proc. Natl. Acad. Sci. U.S.A., 115 (9), pp. 2022-2025, 2018.

Paul, B. K.: Why relatively fewer people died? The case of Bangladesh's Cyclone Sidr. Natural Hazards, 50, 289-304, 2009.

Peltier WR.: Global Glacial Isostasy and the Surface of the Ice-Age Earth: The ICE-5G (VM2) Model and GRACE, Ann. Rev. Earth and Planet. Sci., 32, 111-149, 2004.

Pinardi, N., A. Bonaduce, A. Navarra, S. Dobricic, P. Oddo: The mean sea level equation and its application to the mediterranean sea. J. Climate, 27, 442–447, doi: 10.1175/JCLI-D-13-00139.1, 2014.

Pringle, W. J., Wirasaet, D., Roberts, K. J., and Westerink, J. J.: Global storm tide modeling with ADCIRC v55: unstructured mesh design and performance, Geosci. Model Dev., 14, 1125–1145, https://doi.org/10.5194/gmd-14-1125-2021, 2021.

Pugh, D., and Woodworth, P.: Sea-Level Science: Understanding Tides, Surges, Tsunamis and Mean Sea-Level Changes. Cambridge: Cambridge University Press. doi:10.1017/CBO9781139235778, 2015.

Rajalakshmi PR and H Achyuthan: Climate Change as Observed in the Bay of Bengal. Journal of Climate Change, 7(3), 69-82. DOI 10.3233/JCC210020, 2021.

Ren, H. R., Li, G. S., Cui, L. L., Zhang, Y., and Ouyang, N. L.: Wave Climate Changes in Bohai Sea Related to the East Asian Circulation Oscillations over the Last Sixty Years. Climatic and Environmental Research, 21(4), 490-502, 2016.

Sahoo, B., and Bhaskaran, P. K.: Assessment on historical cyclone tracks in the Bay of Bengal, east coast of India. Int. J. Climatol. 36, 95–109. doi:10.1002/joc.433, 2016.

Schumacher, M., King, M., Rougier, J., Sha, Z., Khan, S.A., & Bamber, J.L.: A new global GPS data set for testing and improving modelled GIA uplift rates. Geophysical Journal International, 214(3), 2164–2176. https://doi.org/10.1093/gji/ggy235, 2018.

https://doi.org/10.5194/egusphere-2025-1763
Preprint. Discussion started: 10 June 2025
© Author(s) 2025. CC BY 4.0 License.

Shimura, T., Pringle, W. J., Mori, N., Miyashita, T., and Yoshida, K.: Seamless projections of global storm surge and ocean waves under a warming Climate. Geophysical Research Letters, 49, e2021GL097427. https://doi.org/10.1029/2021GL097427, 2022.

Singh, K., Panda, J., Sahoo, M., and Mohapatra, M.: Variability in Tropical Cyclone Climatology over North Indian Ocean during the Period 1891 to 2015. Asia-Pacific J. Atmos. Sci. 55, 269–287. doi:10.1007/s13143-018-0069-0, 2019.

State Oceanic Administration: China Marine Hazard Bulletin in 2006, 2006.

State Oceanic Administration: China Marine Hazard Bulletin in 2007, 2007.

State Oceanic Administration: China Marine Hazard Bulletin in 2008, 2008.

Taburet G., Ghantous, M., Lefèvre, F.: C3S Sea level Version DT2021: Algorithm Theoretical Basis Document. Issue 1.2. E.U. Copernicus Climate Change Service. Document ref. WP2-FDDP-2022-03_C3S2-Lot3_ATBD-of-vDT2021-SeaLevel-products_v1.2., 2023.

Tadesse M, Wahl T and Cid A.: Data-Driven Modeling of Global Storm Surges. Front. Mar. Sci. 7: 260. doi: 10.3389/fmars.2020.00260, 2020.

The Climate Change Initiative Coastal Sea Level Team: Coastal sea level anomalies and associated trends from Jason satellite altimetry over 2002–2018. Sci Data 7, 357). https://doi.org/10.1038/s41597-020-00694-w, 2020.

Tiggeloven, T., Couasnon, A., van Straaten, C., Muis, S., and Ward, P. J.: Exploring deep learning capabilities for surge predictions in coastal areas. Scientific Reports, 11(1), 1-15. [17224]. https://doi.org/10.1038/s41598-021-96674-0, 2021.
UN (2017). The Ocean Conference 2017, Factsheet. Accessed 6 March 2023: https://www.un.org/sustainabledevelopment/wp-content/uploads/2017/05/Ocean-fact-sheet-package.pdf

van den Hurk, B., Pinardi, N., Kiefer, T., Larkin, K., Manderscheid, P., and Richter, K. (Eds.): Sea Level Rise in Europe:1st Assessment Report of the Knowledge Hub on Sea Level Rise (SLRE1), Copernicus Publications, State Planet, 3-slre1, https://doi.org/10.5194/sp-3-slre1, 2024.

Vitousek, S., Barnard, P. L., Fletcher, C. H., Frazer, N., Erikson, L., and Storlazzi, C. D.: Doubling of coastal flooding frequency within decades due to sea-level rise. Sci. Rep. 7:1399. doi: 10.1038/s41598-017-01362-7, 2017.

Xue, YQ, Zhang, Y, Ye, SJ et al.: Land subsidence in China. Environ Geol 48, 713–720. https://doi.org/10.1007/s00254-005-0010-6, 2005.

Wahl, T., Haigh, I. D., Nicholls, R. J., Arns, A., Dangendorf, S., Hinkel, J., et al.: Understanding extreme sea levels for broad-scale coastal impact and adaptation analysis. Nat. Commun. 8:16075. doi: 10.1038/ncomms16075, 2017.

Wang, H., Li, W.S., Xiang, W.X.: Sea level rise along China coast in the last 60 years. Acta Oceanol. Sin., 2022, Vol. 41, No. 12, P. 1–9. https://doi.org/10.1007/s13131-022-2066-5, 2022.

https://doi.org/10.5194/egusphere-2025-1763
Preprint. Discussion started: 10 June 2025
© Author(s) 2025. CC BY 4.0 License.

Woodworth and Player: The Permanent Service for Mean Sea Level: An Update to the 21stCentury, 2003.

Zhang, Y., Guo, J., & Che, Z.: Discussion on evaluating the vulnerability of storm surge hazard bearing bodies in the coastal areas of Wenzhou. Frontiers of Earth Science, 9, 300-307, 2015.

Zhang, H. and Sheng, J.: Examination of extreme sea levels due to storm surges and tides over the northwest Pacific Ocean, Continental Shelf Research, 93, pp. 81–97. doi:10.1016/j.csr.2014.12.001, 2015.

Zhao, R., Zhu, X., & Park, J.: Near 5-Day Nonisostatic Response to Atmospheric Surface Pressure and Coastal-Trapped Waves Observed in the Northern South China Sea, Journal of Physical Oceanography, 47(9), 2291-2303. https://journals.ametsoc.org/view/journals/phoc/47/9/jpo-d-17-0013.1.xml, 2017.

Zheng, C. W., & Li, C. Y.: Variation of the wave energy and significant wave height in the China Sea and adjacent waters. Renewable and Sustainable Energy Reviews, 43, 381-387, 2015.

Zhou, Y., Yang, S., Luo, J., Ray, J., Huang, Y., Li, J.: Global Glacial Isostatic Adjustment Constrained by GPS Measurements: Spherical Harmonic Analyses of Uplifts and Geopotential Variations. *Remote Sens. 12*, 1209. https://doi.org/10.3390/rs12071209, 2020.

Zhu, J.Q., Yang, Y., Yu, j., and Gong, X. L.: Land subsidence of coastal areas of Jiangsu Province, China: historical review and present situation Proc. IAHS, 372, 503–506, 2015 proc-iahs.net/372/503/2015/ doi:10.5194/piahs-372-503-2015, 2015.